Nuclear Engineering and Technology 49 (2017) 1326–1338

Contents lists available at ScienceDirect

Nuclear Engineering and Technology

journal homepage: www.elsevier.com/locate/net

Original Article

MC21/CTF and VERA multiphysics solutions to VERA core physics benchmark progression problems 6 and 7☆

Daniel J. Kelly III [a, *], Ann E. Kelly [a], Brian N. Aviles [a], Andrew T. Godfrey [b], Robert K. Salko [b], Benjamin S. Collins [b]

[a] Bechtel Marine Propulsion Corporation, P.O. Box 1072, Schenectady, NY, 12301-1072, USA
[b] Oak Ridge National Laboratory, 1 Bethel Valley Road, Oak Ridge, Tennessee, 37830, USA

ARTICLE INFO

Article history:
Received 30 May 2017
Accepted 11 July 2017
Available online 10 August 2017

Keywords:
CTF
MC21
MPACT
Multiphysics
VERA

ABSTRACT

The continuous energy Monte Carlo neutron transport code, MC21, was coupled to the CTF subchannel thermal-hydraulics code using a combination of Consortium for Advanced Simulation of Light Water Reactors (CASL) tools and in-house Python scripts. An MC21/CTF solution for VERA Core Physics Benchmark Progression Problem 6 demonstrated good agreement with MC21/COBRA-IE and VERA solutions. The MC21/CTF solution for VERA Core Physics Benchmark Progression Problem 7, Watts Bar Unit 1 at beginning of cycle hot full power equilibrium xenon conditions, is the first published coupled Monte Carlo neutronics/subchannel T-H solution for this problem. MC21/CTF predicted a critical boron concentration of 854.5 ppm, yielding a critical eigenvalue of 0.99994 ± 6.8E-6 (95% confidence interval). Excellent agreement with a VERA solution of Problem 7 was also demonstrated for integral and local power and temperature parameters.

1. Introduction

Monte Carlo reactor physics codes coupled with subchannel thermal-hydraulics (T-H) codes are becoming more common for the solution of large-scale nuclear reactor problems [1–14]. These complement the growing number of coupled deterministic transport reactor physics/subchannel T-H codes applied to similar systems-level reactor problems. This paper describes the coupling of the continuous energy Monte Carlo code, MC21 [15], to the subchannel T-H code, CTF [16], which is part of the Consortium for Advanced Simulation of Light Water Reactors (CASL) Virtual Environment for Reactor Applications (VERA) code system [17,18]. MC21/CTF solutions for CASL VERA Core Physics Benchmark Progression Problems 6 and 7 [19] are presented and compared to VERA solutions (MPACT coupled to CTF) of the same benchmark problems.

2. MC21/CTF coupling

Previous work reported the coupling of MC21 and COBRA-IE [20] for the analysis of a hot-full-power (HFP) pressurized water reactor assembly [1]. COBRA-IE and CTF share a common COBRA ancestor but have been developed separately. Because CTF is the subchannel T-H code in VERA, it is desirable to couple MC21 and CTF to fully separate differences between neutronics and T-H effects. In this work, MC21 is coupled to CTF using a combination of modules from VERA and in-house Python scripts, as shown in Figs. 1–3 and described below.

Input processing for VERA is performed using the VERAIn common input parser and VERA processing tools [21] (Fig. 1) to generate CTF model input and geometry information needed to map results between MC21 and CTF. CTF input is generated for the complete model using that VERA input file. Although this section describes the Problem 7 benchmark, a ¼-core model of Watts Bar Unit 1, the Problem 6 benchmark model with a single assembly (and single CTF input/output file) was also run using the same process with different input arguments.

The MC21 model input file is processed with the Physics Unified Modeling and Analysis (PUMA) system, which generates all necessary input files for MC21 execution (Fig. 2). PUMA and MC21 are part of the Common Monte Carlo Design Tool (CMCDT) project

☆ The submittal manuscript has been authored by a contractor of the US Government under contract No. DE-NR-0000031. Accordingly, the US Government retains a nonexclusive, royalty-free license to publish or reproduce the published form of this contribution, or allows others to do so, for US Government purposes.

* Corresponding author.
E-mail address: daniel.kelly@unnpp.gov (D.J. Kelly).

http://dx.doi.org/10.1016/j.net.2017.07.016

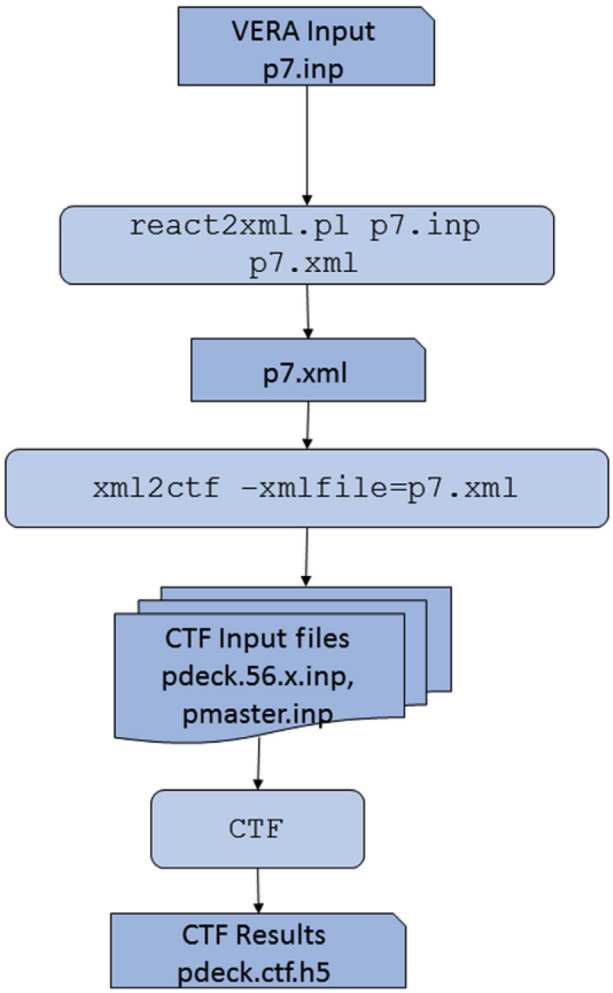

Fig. 1. VERAIn/CTF preprocessing flowchart (blue = VERA codes and files).

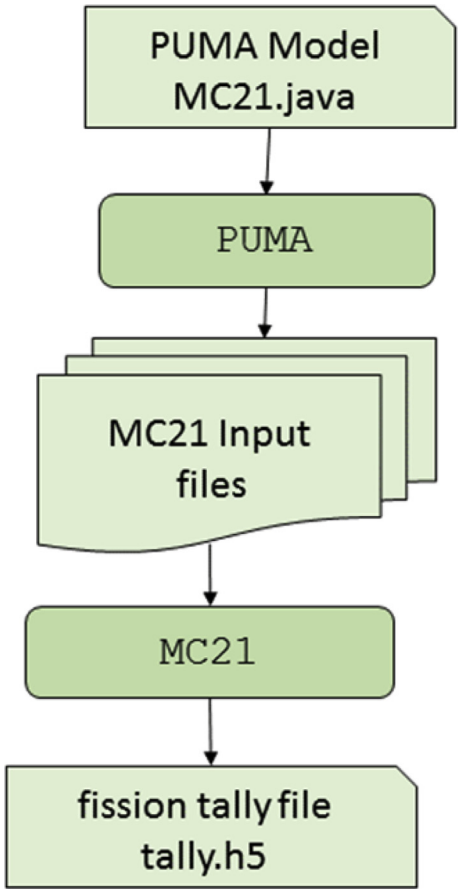

Fig. 2. MC21 preprocessing and initial isothermal job (green = CMCDT codes and files).

at the Naval Nuclear Laboratory [15,22]. MC21 is executed initially with isothermal T-H conditions.

With MC21 and CTF model initialization complete, a converged mutually-consistent neutronics and T-H solution is performed via Picard iteration (Fig. 3). First, the in-house mc21_to_ctf.py script combines geometry information from the CTF model with fission tallies and additional job information from MC21 to compute relative linear heat rate distributions for each assembly. The process uses the CTF HDF5 pdeck.h5 file and the power distribution information is written to the "pin_powers" data set in that file in the correct assembly locations. Second, CTF is then executed using the multistate_cobra external driver program [23] and the newly generated pdeck.h5 file containing the MC21 power distributions, as well as the CTF model generated from the VERAIn file. Third, subchannel temperatures and densities, and fuel rod volume-average temperatures are collected from the CTF HDF5 output by the in-house ctf_to_mc21.py script and translated back to the proper MC21 regions. These temperatures and densities are saved in an MC21 HDF5 file that will be imported in the next execution of MC21. Fourth, MC21 is executed with updated T-H conditions. The Picard iteration in Fig. 3 is repeated until convergence is achieved.

3. Model description

The MC21 model was generated using the PUMA model builder which is part of the CMCDT project [22]. PUMA input is based on a Java input deck, which easily enables the user to build complicated geometries using built-in methods in addition to the many features of the Java programming language. Specifications of the VERA benchmark problems are taken from [19]. New to this work is the restructuring of the PUMA model to more easily facilitate the construction of MC21 models based on the VERA common input file [21]. Building MC21 models with this format simplifies model construction as well as enhances model quality assurance by enabling direct model input comparisons between the corresponding VERA and PUMA/MC21 models. For PUMA to support this type of format, a separate Java class (VERA-Util) was written to handle model construction. At this stage of development, the various VERA input cards such as cell, lattice, axial, and assm_map (to name a few) are reformatted to work within the PUMA framework. Ideally, a PUMA translator would read these cards directly. For both VERA Benchmark Problems 6 and 7, the 2D lattices were constructed using octant-symmetry. The corresponding VERA input files are available from CASL.

An example extracted from the PUMA input file to construct a pin cell and corresponding fuel lattice is shown below.

```
Figure f1 = VERAUtil.makePinCell("F1", "0.4096 0.418 0.475 / u21 he zirc4");
```

This line describes the various concentric rings as well as the materials to be assigned to each region. The portion of code that specifies input required to construct a fuel lattice in PUMA using octant symmetry with the VERAUtil class is shown below.

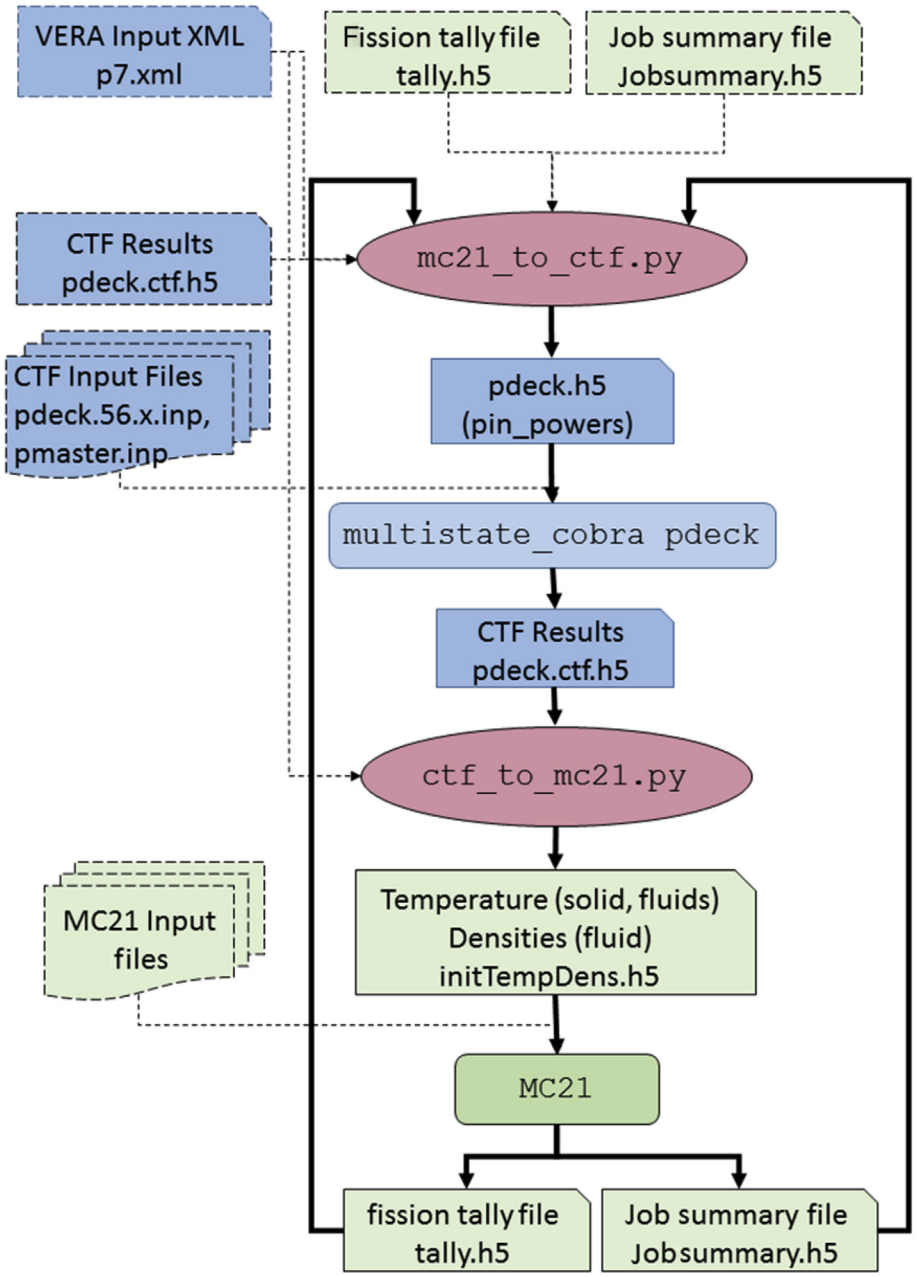

Fig. 3. MC21/CTF Picard iteration flowchart (blue = VERA codes and files, green = CMCDT codes and files, magenta = in-house scripts), dashed lines = files generated in pre-processing steps.

```
Figure[] fig26 = {
        g4,
        f1, f1,
        f1, f1, f1,
        g4, f1, f1, g4,
        f1, f1, f1, f1, f1,
        f1, f1, f1, f1, f1, g4,
        g4, f1, f1, g4, f1, f1, f1,
        f1, f1, f1, f1, f1, f1, f1, f1,
        f1, f1, f1, f1, f1, f1, f1, f1, f1};
Overlay lat26 = VERAUtil.makeLattice("LAT26", fig26)
```

In a standard MC21 PUMA model, each unit cell is constructed from five regions consisting of two squares (the outer square is either spacer grid material or coolant and the inner square is subchannel coolant) and three concentric circles (clad, gap, and fuel). For a thermal-hydraulic feedback model, 11 regions are required since the grid and coolant regions are each subdivided into quadrants (Fig. 4). In addition, the thermal-hydraulic feedback case requires that the respective quadrant from one pin cell share a common "attribute" with the adjoining quadrants in the neighboring pin cell so that a compatible subchannel is defined to interface with the CTF model (Fig. 5). Fuel pins are specified as a complete pin and a separate attribute is assigned to these regions.

The "attribute" mentioned above is a powerful feature of PUMA where specific properties, called attributes, can be assigned to geometric figures during model creation such that a specific set of figures can be grouped together for the purpose of edits and/or material assignments. As part of the internal temperature feedback capabilities of MC21 [15], specific attributes called "source" and "sink" are used to specify power generating regions (sources) and coolant regions (sinks). In the MC21 input files, specific input is given for these two attributes in addition to the standard "region id" and "material id". In addition, the temperature feedback capability of MC21 specifies a unique file format whereby the user can specify the temperature of the sources (i.e., fuel pins) and both the temperature and density of the sinks (i.e., coolant regions) to achieve the effects of temperature feedback on MC21 material number densities and cross sections. These input files and features of MC21

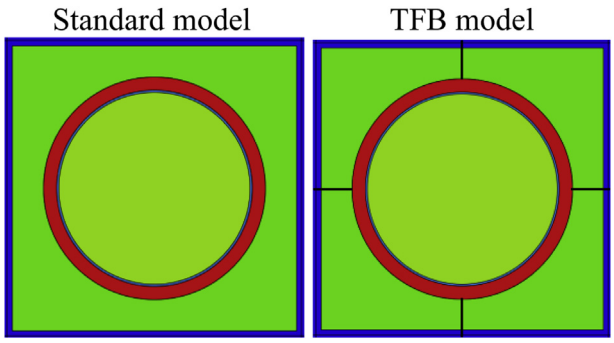

Fig. 4. MC21 PUMA description of pin cell geometry.

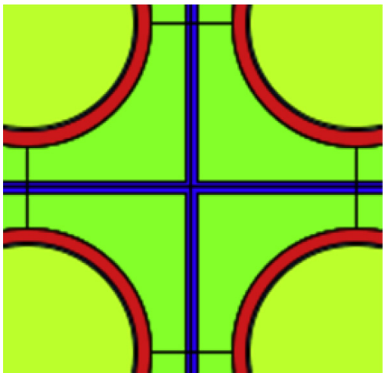

Fig. 5. MC21 PUMA Description of thermal-hydraulic feedback subchannel geometry.

and PUMA allow MC21 to be coupled to external T-H codes such as CTF. In the current MC21/CTF coupling methodology, CTF returns volume-average fuel temperature within each pin for each axial segment to the corresponding MC21 region at that elevation. Internal CTF conduction models and properties [16] were used for both MC21/CTF and VERA in this study.

4. Results

4.1. VERA Core Physics Benchmark Problem 6

VERA Core Physics Benchmark Problem 6 is a pressurized water reactor fuel assembly at HFP conditions [19]. Problem 6 was simulated without guide tube heating using MC21/CTF to demonstrate that coupling of MC21 and CTF using the process described in Section II was working properly. MC21/CTF results are compared with updated MC21/COBRA-IE and VERA solutions from [1]. The MC21 and CTF assembly geometry is described in [1,19]. MC21 uses cross sections from ENDF/B-VII.1, with nonwater material cross sections ranging from 500 K to 1,600 K in 50 K increments up to 900 K and 100 K increments thereafter, and water cross sections ranging from 500 K to 650 K at 10 K intervals. MPACT employs a 51 energy group cross-section library based on ENDF/B-VII.1 data with subgroup parameters to capture self-shielding effects. Methods for treating resonance upscatter were not employed in either MC21 or MPACT in this analysis. All MC21 uncertainties and relative uncertainties are based on 95% confidence intervals.

Nine coupled iterations were simulated to converge MC21 and CTF. Fig. 6 presents the MC21 eigenvalue trajectory during the nine data exchanges. The number of active neutron histories for each data exchange is shown on the right axis and increases from 200 million histories at the first data exchange to 2 billion histories for data exchanges 5 through 9 (200 active generations of 10 million neutrons per generation preceded by 50 discarded generations). Two billion histories were adequate to reduce uncertainties in local pin power $< 0.7\%$ [1]. The MC21 eigenvalue is converged at data exchange 5 when the two billion active neutron history value is reached.

Local subchannel coolant temperature, average fuel rod temperature, and pin linear heat rate convergence metrics, as measured by the L_2 and L_∞ norms with respect to their respective final (exchange index 9) distributions, are presented in Figs. 7–9. As was done in [1], the L_2 norm for coolant temperature was normalized by the square root of the number of subchannel regions (4,410), and the L_2 norms for fuel temperature and pin linear heat rate were normalized by the square root of the number of fuel regions (3,528). Thus, the following norms are used to monitor convergence in the CTF solution ($N = 9$ in Figures 6 and 7):

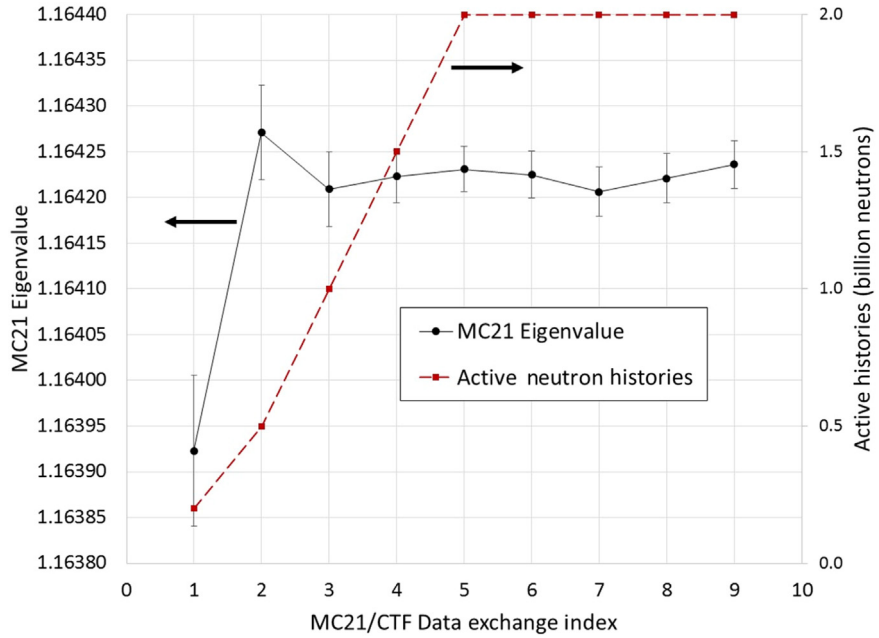

Fig. 6. MC21 eigenvalue and number of active neutron histories during MC21/CTF data exchanges.

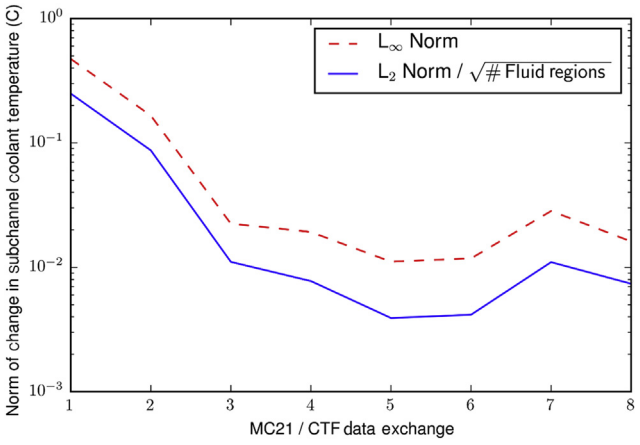

Fig. 7. CTF convergence metrics for subchannel coolant temperature during MC21/CTF data exchanges.

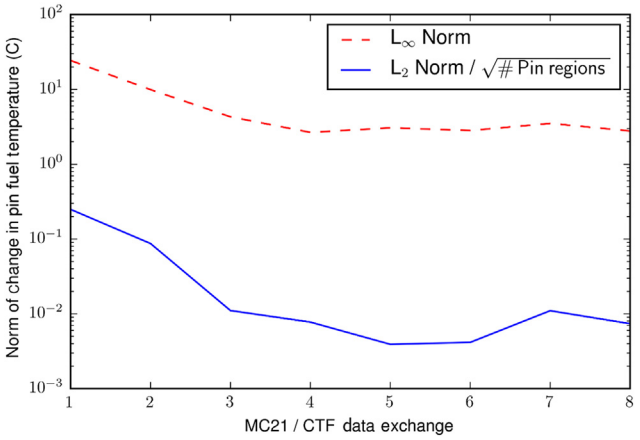

Fig. 8. CTF convergence metrics for fuel temperature during MC21/CTF data exchanges.

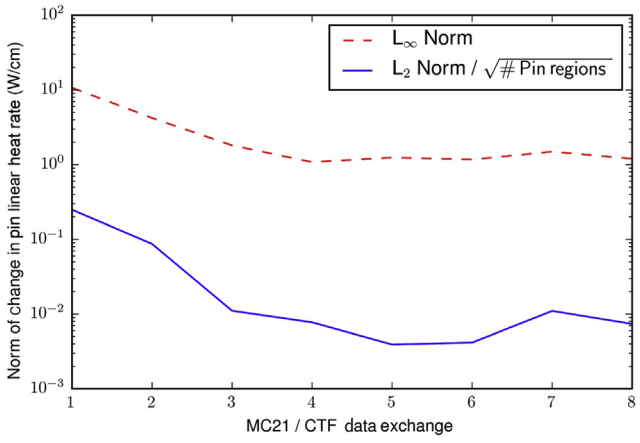

Fig. 9. CTF convergence metrics for pin linear heat rate during MC21/CTF data exchanges.

L_∞ norm of fuel temperature:

$$\left\| \boldsymbol{T}_f^n - \boldsymbol{T}_f^N \right\|_\infty \quad \text{for } n = 1, N-1 \tag{1}$$

L_2 norm of fuel temperature:

$$\frac{\left\| \boldsymbol{T}_f^n - \boldsymbol{T}_f^N \right\|_2}{\sqrt{\#\ Fuel\ regions}} \quad \text{for } n = 1,\ N-1 \tag{2}$$

L_∞ norm of relative change in coolant density:

$$\left\| \frac{\boldsymbol{\rho}_c^n - \boldsymbol{\rho}_c^N}{\boldsymbol{\rho}_c^N} \right\|_\infty \quad \text{for } n = 1,\ N-1 \tag{3}$$

L_2 norm of relative change in coolant density:

$$\frac{\left\| \frac{\boldsymbol{\rho}_c^n - \boldsymbol{\rho}_c^N}{\boldsymbol{\rho}_c^N} \right\|_2}{\sqrt{\#\ Coolant\ regions}} \quad \text{for } n = 1,\ N-1 \tag{4}$$

where,

$\boldsymbol{T}_f^n$ = vector of local fuel temperatures for data exchange index n,

$\boldsymbol{T}_f^N$ = vector of local fuel temperatures at the final data exchange N,

$\boldsymbol{\rho}_c^n$ = vector of local subchannel coolant densities for data exchange index n, and

$\boldsymbol{\rho}_c^N$ = vector of local subchannel coolant densities at the final data exchange N.

These norms also indicate that the coupled MC21/CTF solution is converged at data exchange 5, as local coolant temperatures are within 0.02°C, local fuel temperatures are within 3°C, and local pin linear heat rates are within 2 W/cm of their final data exchange values, respectively.

Table 1 presents calculated eigenvalues for the three code systems. MC21/CTF and MC21/COBRA-IE produce statistically-equivalent eigenvalues. Agreement within 100 pcm is considered to be good agreement.

Table 1
Calculated eigenvalues for CASL P6 ¼-assembly.

Code System	Eigenvalue (95% CI)	Difference (pcm)
MC21/COBRA-IE	1.16424 (2.6E−05)	Reference
MC21/CTF	1.16424 (2.6E−05)	0
MPACT/CTF	1.16361	−63

CI, confidence interval.

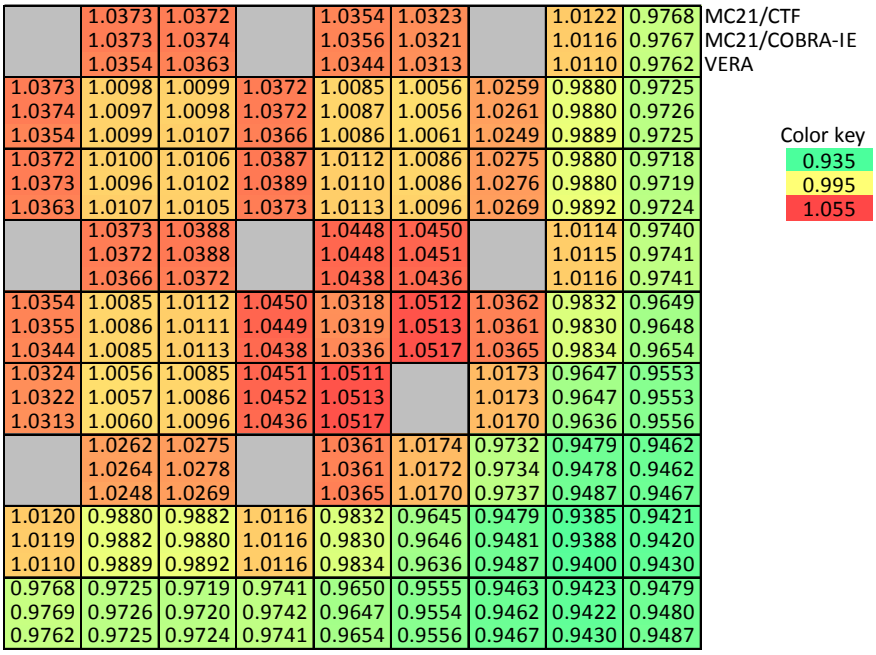

Fig. 10. Axially-integrated ¼-assembly normalized pin fission rate comparison, VERA Problem 6.

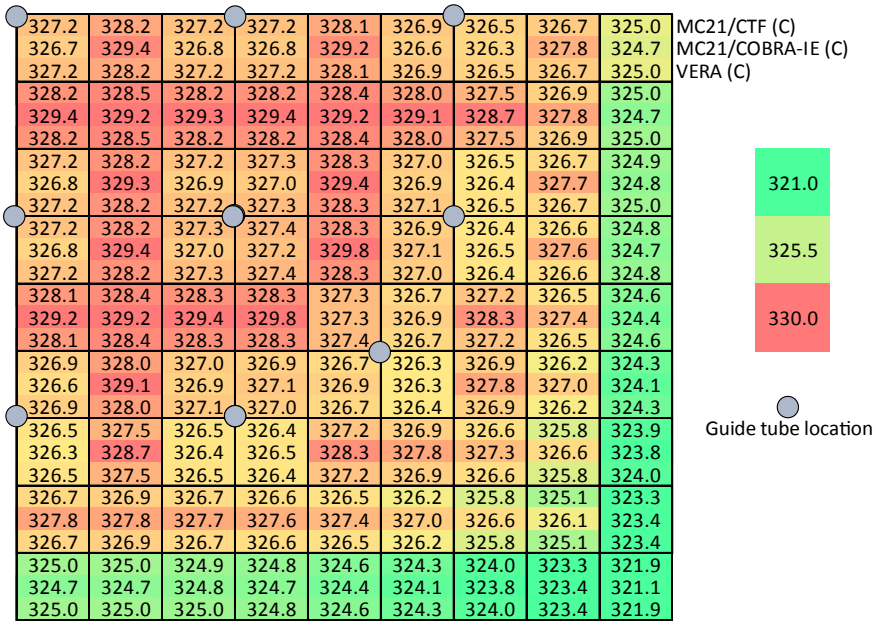

Fig. 11. Subchannel exit coolant temperature comparison, VERA Problem 6.

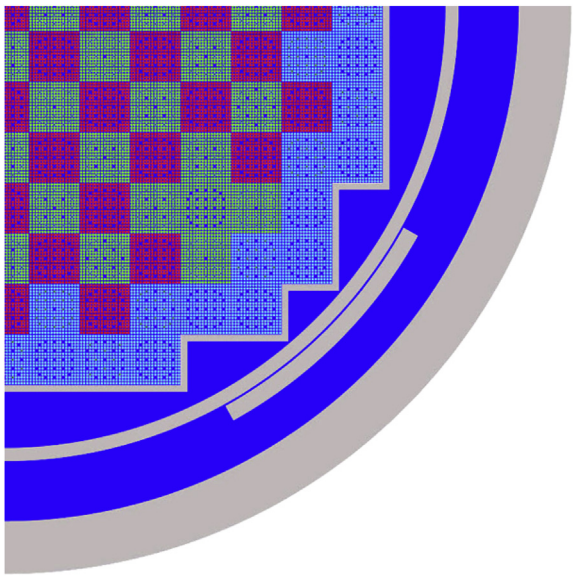

Fig. 12. PUMA visualization of ¼-core MC21 model for VERA Problem 7.

Fig. 10 presents axially-integrated ¼-assembly normalized pin fission rates, and Fig. 11 presents subchannel exit coolant temperatures for all three code systems. MC21/CTF produces results nearly identical to MC21/COBRA-IE and consistent with VERA. Focusing on MC21/CTF comparisons with VERA (the subject of this study), the maximum differences in axially-integrated pin power are −0.21% in pin (9,10) and +0.17% in pin (13,13) with a root mean square (RMS) difference of 0.09%. These differences are outside of the uncertainties in MC21 axially-integrated relative pin power (< 0.03% at two billion active neutron histories), and thus are statistically significant. Subchannel exit coolant temperatures provide a measure of radial pin power sharing for VERA and MC21/CTF, and they agree within ± 0.1°C with an RMS difference of 0.02°C.

A comparison of MC21/CTF and VERA local results for the 3D ¼-assembly model yields an RMS difference of 0.1°C for all subchannel coolant temperature regions (9% of all subchannel coolant temperatures agree within the 0.01°C coolant temperature convergence criterion of CTF in this analysis), an RMS difference of 4.4°C for all fuel pin volume-average temperature regions (39% of all volume-average fuel temperatures agree within the 3°C fuel temperature convergence criterion of CTF in this analysis), and an RMS difference of 0.053 in normalized fission rate for all fuel rod power regions (fission rates are normalized such that the average fission rate is 1.0).

Table 2
MC21/CTF running strategy.

Picard iterations	Actions	Boron (ppm)	Active histories (generation size)	k_{calc} (95% CI)
1	Fixed boron, isothermal, eqXe	900.0	50 million (500,000)	1.01133 (1.8E−4)
2	Boron search, T/H feedback, eqXe	859.7	100 million (1 million)	0.99989 (1.2E−4)
3	Boron search, T/H feedback, eqXe	852.3	100 million (1 million)	1.00003 (1.0E−4)
4	Fixed boron, T/H feedback, eqXe	852.3	500 million (1 million)	1.00031 (4.8E−5)
5	Fixed boron, T/H feedback, eqXe	854.5	30 billion (4 million)	0.99994 (6.8E−6)

CI, confidence interval.

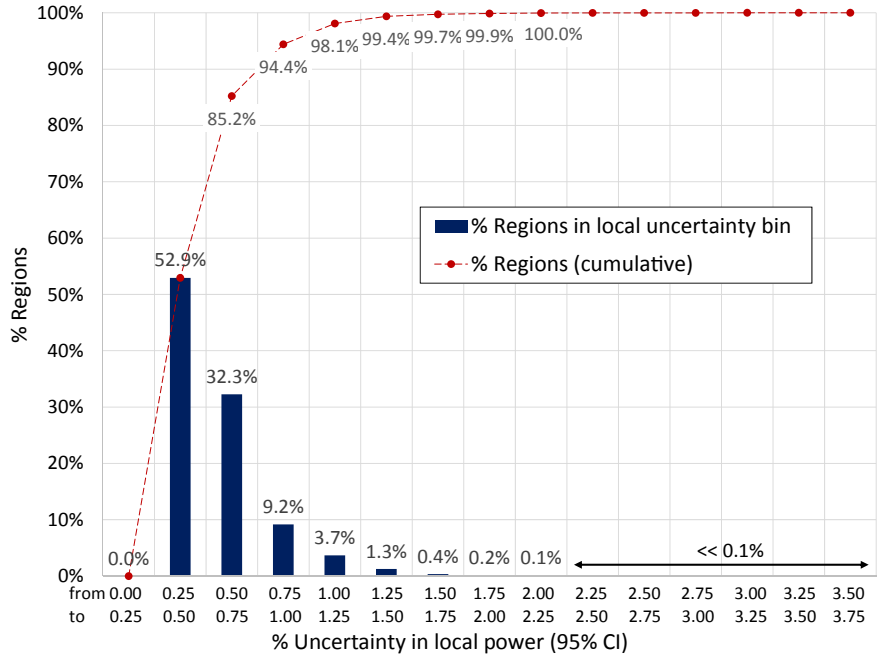

Fig. 13. Distribution of MC21 relative uncertainty in relative power density for VERA Problem 7, 30 billion neutrons. CI, confidence interval.

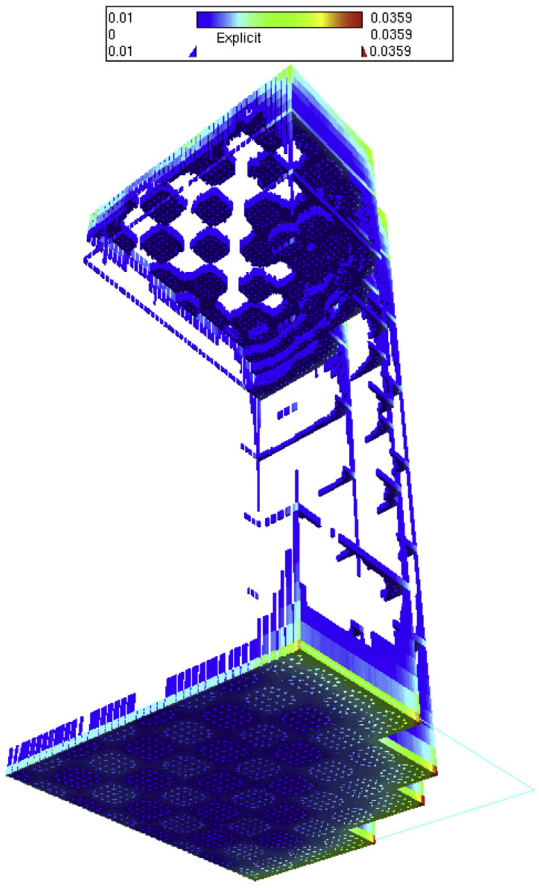

Fig. 14. Distribution of MC21 relative uncertainties in relative power density > 1%, VERA Problem 7, 30 billion neutrons.

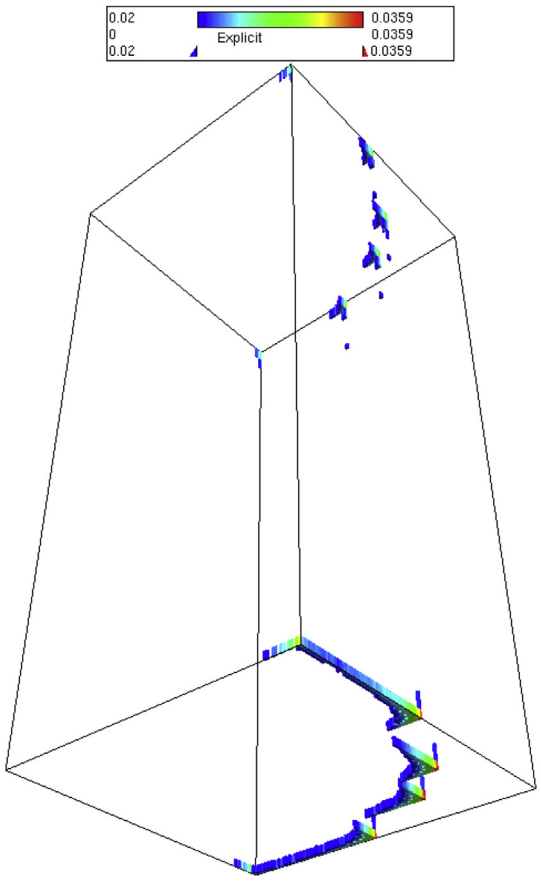

Fig. 15. Distribution of MC21 relative uncertainties in relative power density > 2%, VERA Problem 7, 30 billion neutrons.

4.2. VERA Core Physics Benchmark Problem 7

VERA Core Physics Benchmark Problem 7 represents Watts Bar Nuclear Unit 1 at beginning of cycle, HFP, equilibrium xenon conditions [19], with different fuel enrichments of 2.11% (red), 2.619% (green), and 3.10% (blue), respectively, as shown in Fig. 12. The cross section libraries for MC21 and MPACT for Problem 7 are identical to Problem 6, as described in Section 4.1. In this analysis, all central instrument tubes were replaced with guide tubes to enable ¼-core symmetry. Instrument tubes will be reinstated when future comparisons with flux maps are performed. A reactivity sensitivity study of replacing instrument tubes with guide tubes was performed with VERA, indicating that guide tubes are worth ~4 ppm of boron (~40 pcm).

MPACT was executed using the 2D/1D technique with transport-corrected P_0 2D method of characteristics (MOC) in the radial planes and SP_3 in the axial direction. Temperature and density changes are monitored to determine if the subgroup calculation needs to be re-executed to obtain new shielding parameters for cross section generation.

4.2.1. MC21/CTF running strategy

MC21 was executed using the critical boron search feature of MC21 at equilibrium xenon conditions with full T-H feedback using fuel and coolant temperatures and coolant densities from CTF. Table 2 describes the running strategy and results for MC21/CTF during the five Picard iterations. The goal was to compute critical boron such that MC21's eigenvalue was within ± 10 pcm of unity. Critical boron searches were performed in iterations 2 and 3. The critical boron concentration search range for MC21 was set from 700 ppm to 900 ppm, and MC21 automatically performs partial spatial solutions until the eigenvalue is within a user-specified tolerance (± 10 pcm in this study), at which time MC21 performs a

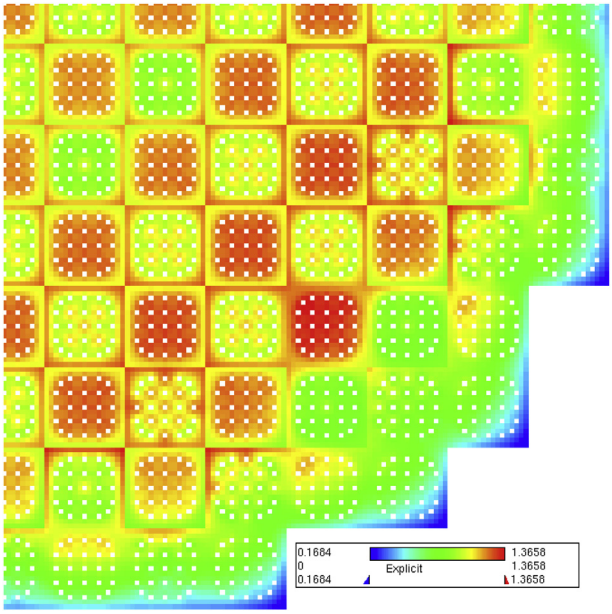

Fig. 16. MC21 axially-integrated relative pin power distribution. Minimum = 0.1684, maximum = 1.3658.

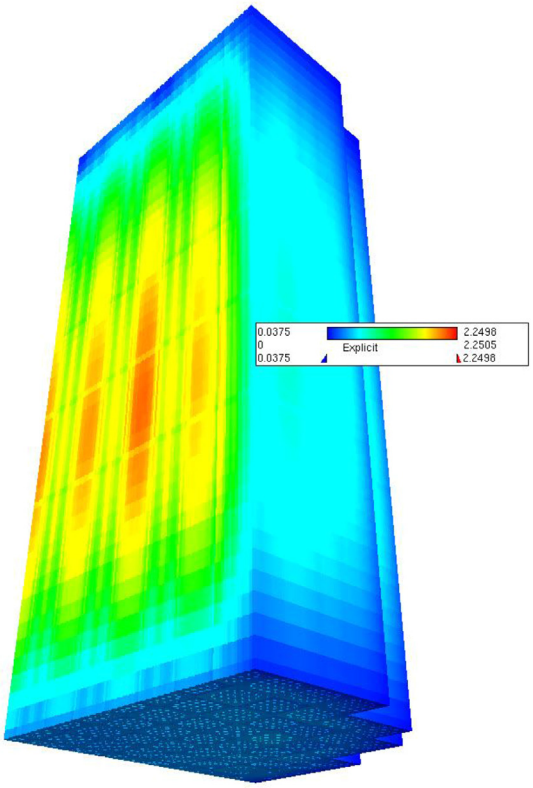

Fig. 17. MC21 3D relative pin power distribution, VERA Problem 7.

full spatial solution. Equilibrium xenon was updated every five generations (user specified). Note that in iteration 4, as the number of active histories increased, the more tightly-converged power solution affected the temperature distributions and caused the calculated eigenvalue to stray outside the ± 10 pcm target set by the earlier critical boron searches. Based on MC21's estimate of boron sensitivity from these earlier iterations (~10.3 pcm/ppm), boron concentration was re-adjusted prior to iteration 5. Iteration 5 was then executed as a restart from the iteration 4 solution with 30 billion active neutron histories (7,500 active generations of 4 million neutrons/generation, 50 discarded generations) with the goal of driving the uncertainty on local pin power to ~2%, based on [22]. No variance reduction techniques were employed in this study. For the fifth Picard iteration, MC21 required 164 wall clock hours (6.8 days) using 32 nodes containing two 16-core Intel Xeon E5-2683v4 2.1 GHz (Broadwell) processors (1,024 total cores). VERA execution took 57 min using 464 cores on Idaho National Laboratory's Falcon computer (Intel Xeon E5-2680v3 2.5 GHz processors).

4.2.2. Select MC21/CTF and VERA comparisons

From Table 2, a final critical boron concentration of 854.5 ppm resulted in an MC21 eigenvalue of 0.99994 ± 6.8E−6 [95% confidence interval (CI)]. VERA computes a critical boron concentration of 853.7 ppm for the target eigenvalue of 1.0. Agreement between the two codes is < 1 ppm, and excellent agreement is considered to be within 5 ppm (~50 pcm) for this parameter.

Fig. 13 presents the relative uncertainty in MC21 relative power density after Iteration 5 for all 628,572 mesh tally regions in the ¼-core model in 0.25% resolution bins. At 30 billion active histories, the majority of local power regions (52.9%) have relative uncertainties < 0.5%, 94.4% of all regions have relative uncertainties < 1.0%, and 99.9% of all regions have relative uncertainties less than 2% (the target for this study). The average relative uncertainty is 0.56%. Considering only local power regions with a relative power > 1.0, the maximum relative uncertainty is 1.1%, and the average uncertainty for these regions is 0.43%.

As expected, the regions with the highest local power uncertainties occur in the top and bottom few axial planes, primarily near the core periphery. This is demonstrated in Fig. 14 and Fig. 15, which shows regions with relative uncertainties >1% and >2%, respectively, from a visual perspective at the bottom corner of the core. The maximum relative uncertainty is 3.59% in the first axial plane of pin (17,17) in Assembly B-13, and the minimum relative uncertainty of 0.32% occurs at axial plane 18 (125.419–133.484 cm)

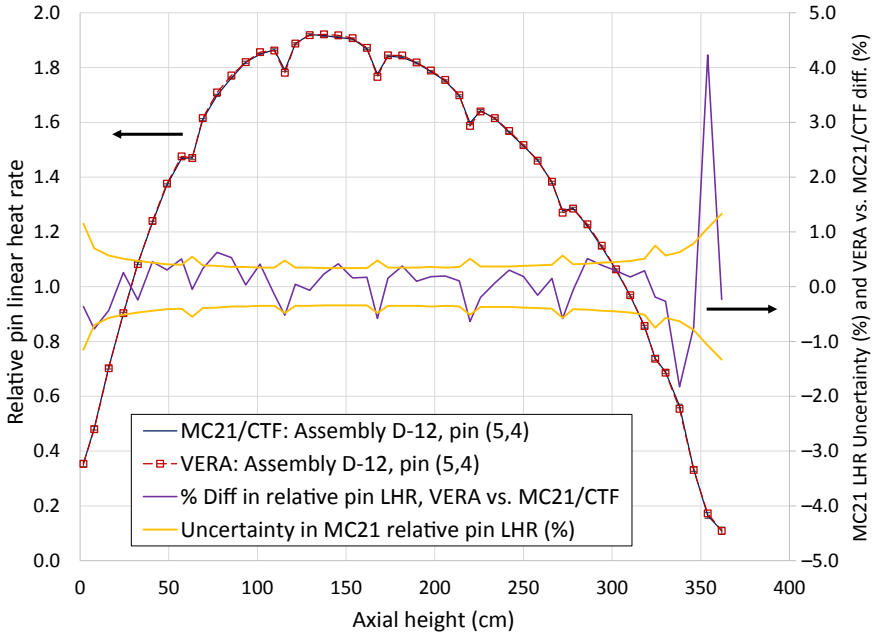

Fig. 18. Axial relative LHR for pin (5,4) in assembly D-12 (y1-axis), and VERA versus MC21/CTF % difference shown with MC21 uncertainty in relative LHR (%) (y2-axis), VERA Problem 7. LHR, linear heat rate.

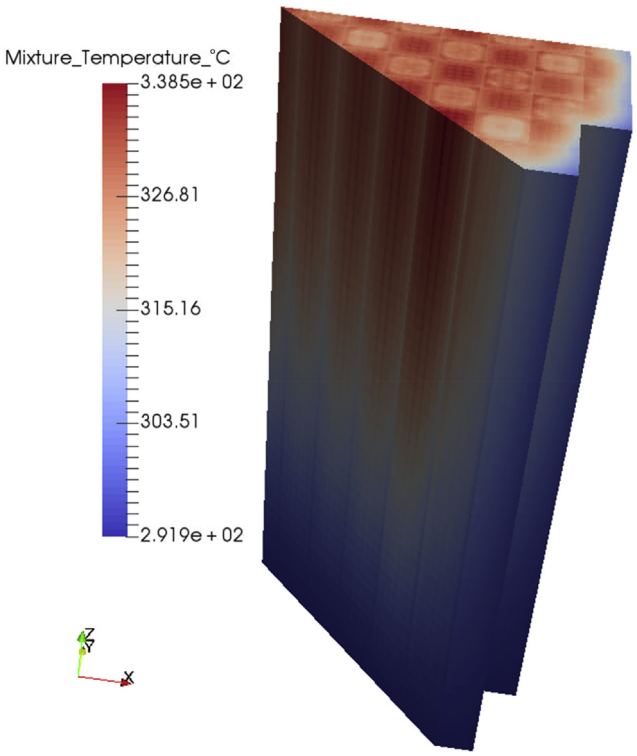

Fig. 19. Three-dimensional octant view of CTF subchannel temperature distribution for MC21/CTF, VERA Problem 7.

in pin (6,6) in Assembly D-10. The very few regions with uncertainties >2% are confined to the outer few pins in the two top and bottom axial planes (Fig. 15). Also note from Fig. 14 that the core periphery regions with smaller volumes in planes containing spacer grids also have slightly higher uncertainties than surrounding regions.

Fig. 16 presents MC21 axially-integrated relative pin power. The MC21 maximum relative pin power of 1.3658 occurs in pin (4,5) in Assembly D-12. VERA predicts the maximum power in the same pin with a value of 1.3670, a difference of 0.09%. MC21/CTF predicts the pin with the smallest relative power to be 0.1684 for pin (17,17) in Assembly C-14. VERA predicts a minimum pin relative power value of 0.1673 in the same pin, a −0.7% difference.

Fig. 17 presents a 3D view of the relative pin power distribution from MC21/CTF. Maximum local power peaking on this tally mesh (pin resolved, 49 axial elevations) is 1.9198 with a relative uncertainty of 0.34%, occurring at axial plane 18 (125.419–133.484 cm) in pin (5,4) in Assembly D-12. For VERA, the maximum local power peaking value of 1.9214 occurs in the same pin one axial elevation higher (133.484–141.55 cm), a difference of 0.08%. This agreement is well within MC21's local relative pin power uncertainty at both axial elevations, as shown in the axial relative pin linear heat rate (LHR) comparison for this pin, presented in Fig. 18. Relative uncertainty (95% CI) error bars are shown on the MC21 curve and repeated on the y2-axis. The y2-axis demonstrates that 69% of VERA's relative LHR results fall within the relative uncertainty of the MC21 relative LHR for this pin. A majority of outliers are in low power regions at the top and bottom of the core, and at spacer grid locations.

An octant view of CTF coolant temperatures from MC21/CTF is presented in Fig. 19 showing subchannel T-H fidelity within the core region.

Fig. 20 presents axially-integrated assembly relative power for MC21/CTF and VERA. Assembly powers agree within −0.47%/+0.37%, with an RMS difference of 0.22%. Agreement within ±0.5% is considered excellent agreement. Uncertainties in MC21 axially-integrated assembly relative power for MC21 range from a minimum of 0.01% in Assembly E-11 to a maximum of 0.022% for the ¼-assembly in the corner of the ¼-core model, Assembly H-8. Thus, all differences in MC21/CTF and VERA assembly relative power are statistically significant except for Assembly H-8. Core-average axial power shape comparisons are presented in Fig. 21. Relative uncertainty (95% CI) error bars are shown on the MC21 curve (repeated on the y2-axis) and are < 0.02% for all axial elevations. The poorer MC21 statistics in the top axial plane affects the difference in this low power core region (y2-axis). The RMS difference between VERA and MC21/CTF for the axial relative power is 0.25%. Axial offsets for MC21/CTF and VERA are −11.06% and −11.03%, respectively. Fig. 22 presents assembly-averaged exit temperatures estimated by mass

	H	G	F	E	D	C	B	A	
8	1.1179	1.0302	1.1156	1.0564	1.1571	1.0531	1.0487	0.7558	MC21/CTF
	1.1177	1.0327	1.1160	1.0591	1.1574	1.0547	1.0454	0.7551	VERA
	−0.02%	0.24%	0.04%	0.26%	0.02%	0.15%	−0.32%	−0.09%	% diff (VERA vs. MC21/CTF)
9	1.0299	1.1081	0.9828	1.1475	1.0795	1.1549	1.0119	0.8558	
	1.0327	1.1091	0.9862	1.1490	1.0826	1.1547	1.0122	0.8548	
	0.27%	0.10%	0.34%	0.13%	0.29%	−0.01%	0.02%	−0.11%	
10	1.1148	0.9825	1.1310	1.0740	1.1844	1.1210	1.0552	0.7646	
	1.1160	0.9862	1.1328	1.0778	1.1856	1.1225	1.0517	0.7633	
	0.10%	0.37%	0.15%	0.36%	0.10%	0.13%	−0.33%	−0.17%	
11	1.0556	1.1471	1.0740	1.1798	1.0774	1.1184	0.9865	0.6335	
	1.0591	1.1490	1.0778	1.1809	1.0799	1.1164	0.9854	0.6322	
	0.33%	0.16%	0.35%	0.10%	0.23%	−0.18%	−0.11%	−0.21%	
12	1.1566	1.0793	1.1850	1.0777	1.2377	0.8650	0.8914		
	1.1574	1.0826	1.1856	1.0799	1.2377	0.8639	0.8895		
	0.07%	0.31%	0.05%	0.20%	0.00%	−0.12%	−0.21%		
13	1.0537	1.1557	1.1219	1.1193	0.8654	0.8656	0.6073		
	1.0547	1.1547	1.1225	1.1164	0.8639	0.8629	0.6059		
	0.10%	−0.08%	0.05%	−0.26%	−0.17%	−0.31%	−0.24%		
14	1.0492	1.0128	1.0565	0.9876	0.8923	0.6077			
	1.0454	1.0122	1.0517	0.9854	0.8895	0.6059			
	−0.37%	−0.06%	−0.46%	−0.22%	−0.31%	−0.29%			
15	0.7563	0.8565	0.7653	0.6343					
	0.7551	0.8548	0.7633	0.6313					
	−0.16%	−0.19%	−0.27%	−0.47%					

Color key
0.600
0.900
1.250

Fig. 20. Axially-integrated assembly relative power, MC21/CTF and VERA, Problem 7.

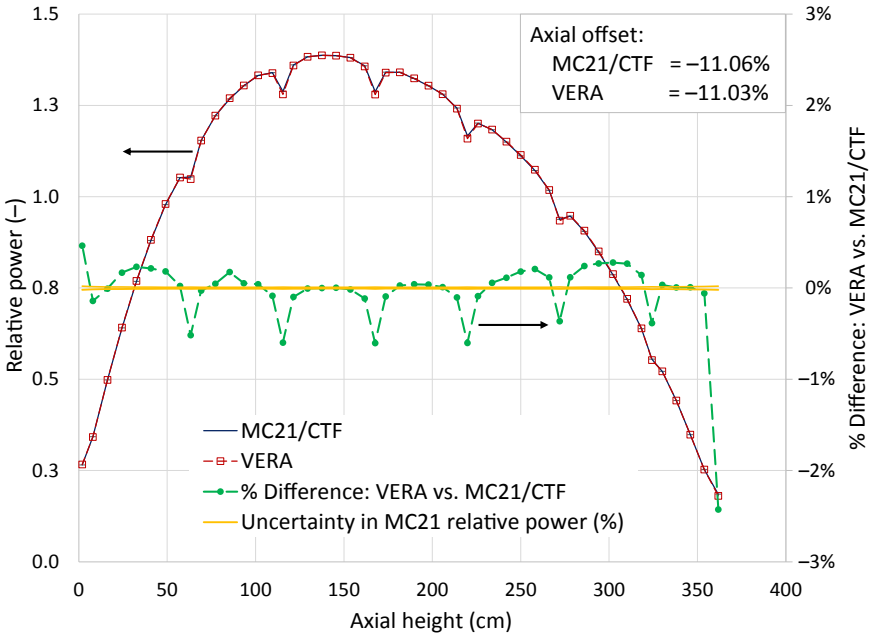

Fig. 21. Core relative axial power and axial offset, MC21/CTF and VERA, Problem 7.

flow weighting the subchannel coolant temperatures in the top axial plane. Assembly exit coolant temperatures agree within −0.2/+0.2°C with an RMS difference of 0.13°C. These comparisons indicate that MC21/CTF and VERA solutions agree for integral assembly-averaged and radially-averaged quantities.

Investigating local thermal-hydraulics quantities also demonstrates a high level of agreement between MC21/CTF and VERA. Fig. 23 is a 2D ¼-core map showing differences (VERA−MC21/CTF) in subchannel exit coolant temperatures. All subchannel exit temperatures agree within −0.25°C/+0.27°C, and a majority (57%) of subchannels agree within ±0.1°C. Assembly F-14 (2.11% enrichment without poison) is the assembly in which VERA computes consistently lower exit coolant temperatures, and Assembly G-10 (2.619% enrichment with 24 Pyrex burnable absorber pins) is the assembly in which VERA predicts the highest subchannel exit temperatures compared to MC21/CTF. There is a checkerboard behavior in the differences between MC21/CTF and VERA for the 2.11% enriched assemblies with no poison pins and the 2.619% enriched assemblies with Pyrex absorber pins. A similar trend was seen in local power comparisons between VERA and the KENO Monte Carlo code for VERA Problem 5 (Watts Bar Unit 1 at hot zero power conditions). At this top axial level, the mean difference between VERA and MC21/CTF is 0.03°C with an RMS difference of 0.13°C. The RMS difference between VERA and MC21/CTF for all subchannel coolant temperature regions in the 3D ¼-core model is 0.08°C, and 25% of all subchannel coolant temperatures agree within the 0.01°C coolant temperature convergence criterion of CTF in this analysis.

	H	G	F	E	D	C	B	A	
8	330.9	327.4	330.8	328.2	332.1	328.2	328.9	318.5	MC21/CTF (C)
	331.0	327.6	330.9	328.4	332.2	328.3	328.8	318.4	VERA (C)
	0.1	0.2	0.1	0.2	0.1	0.1	−0.1	−0.1	Difference (C): VERA - MC21/CTF
9	327.4	330.5	325.9	331.8	329.0	332.2	326.6	321.9	
	327.6	330.7	326.1	332.0	329.2	332.2	326.7	321.8	
	0.2	0.2	0.2	0.2	0.2	0.0	0.1	−0.1	
10	330.8	325.9	331.3	328.8	333.0	330.3	329.2	318.7	Color key
	330.9	326.1	331.4	329.0	333.1	330.4	329.1	318.7	313.00
	0.2	0.2	0.2	0.2	0.1	0.1	−0.1	−0.1	324.00
11	328.2	331.8	328.8	332.9	329.1	331.0	326.0	314.5	335.00
	328.4	332.0	329.0	333.0	329.2	331.0	325.9	314.4	
	0.2	0.2	0.2	0.1	0.1	0.0	−0.1	−0.1	
12	332.1	329.0	333.0	329.1	334.2	322.5	323.0		
	332.2	329.2	333.1	329.2	334.2	322.5	322.9		
	0.1	0.2	0.1	0.1	0.0	0.0	−0.1		
13	328.2	332.2	330.3	331.1	322.6	322.1	313.6		
	328.3	332.2	330.4	331.0	322.5	322.0	313.5		
	0.1	0.0	0.1	−0.1	−0.1	−0.1	−0.1		
14	328.9	326.7	329.2	326.0	323.1	313.6			
	328.8	326.7	329.1	325.9	322.9	313.5			
	−0.1	0.0	−0.1	−0.1	−0.2	−0.1			
15	318.5	321.9	318.8	314.5					
	318.4	321.8	318.6	314.4					
	−0.1	−0.1	−0.2	−0.1					

Fig. 22. Assembly-averaged exit coolant temperature (°C), MC21/CTF and VERA, Problem 7.

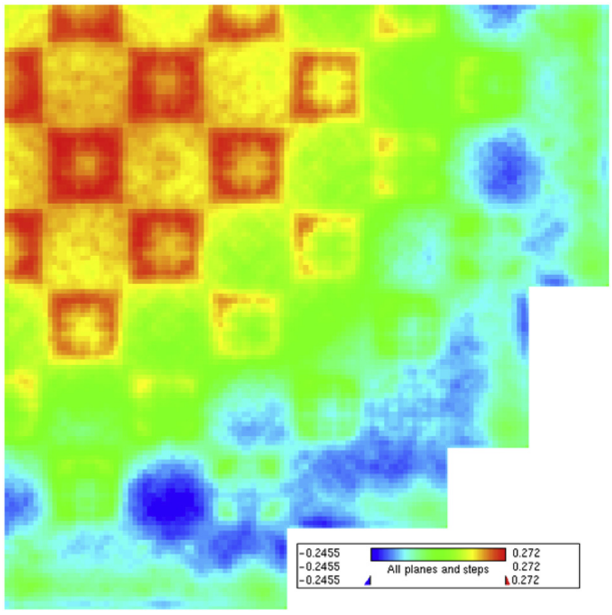

Fig. 23. Difference in subchannel exit coolant temperature (°C), (VERA–MC21/CTF), VERA Problem 7.

Fig. 24 presents a similar temperature difference plot, this time showing differences in local volume-averaged fuel pin temperatures at the axial plane with the maximum fuel temperature (axial plane 19 between 133.484 cm and 141.549 cm). Agreement at this plane is −8.6°C/+7.3°C, with 84% of pin fuel temperatures agreeing within ±3°C (the stopping criterion for fuel temperature convergence in CTF). The mean difference between VERA and MC21/CTF at this axial level is 0.20°C with an RMS difference of 2.1°C. Consistent with the exit coolant temperature map, Assembly F-14 is the assembly with the largest VERA versus MC21/CTF differences. Maximum volume-averaged fuel pin temperature is predicted by MC21/CTF to be 1,065.8°C at pin (5,6) in Assembly D-12. Again, the checkerboard pattern in fuel temperatures between MC21 and MPACT in the 2.11% and 2.6% enriched assemblies is present in the fuel temperatures because of the differences in power distributions. There is also an observable octant tilt resulting from the non-symmetric MC21 solution with only 30 billion neutron histories (also evident in Fig. 20). The RMS difference between VERA and MC21/CTF for all fuel pin volume-average temperature regions in the 3D ¼-core model is 1.9°C, and 88% of all volume-average fuel temperatures agree within the 3°C fuel temperature convergence criterion of CTF in this analysis.

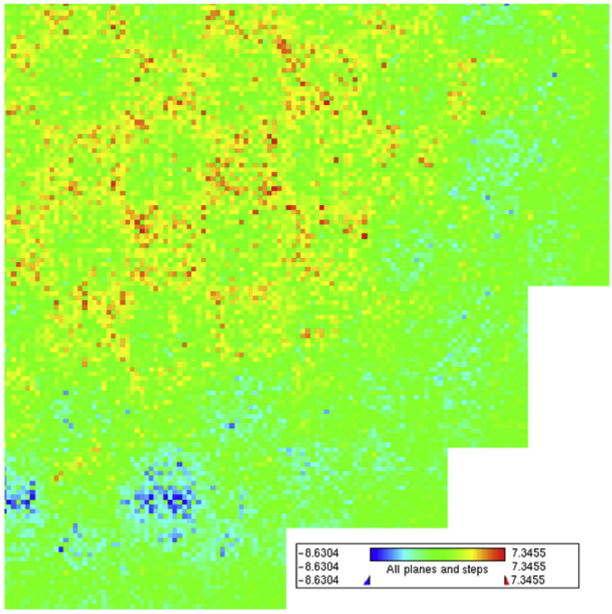

Fig. 24. Difference in volume-averaged fuel pin temperature (°C) at axial plane 19, (VERA–MC21/CTF), VERA Problem 7.

5. Conclusions

The continuous energy Monte Carlo neutron transport code, MC21, was coupled to the CTF subchannel thermal-hydraulics code using a combination of CASL tools and in-house Python scripts. MC21/CTF solutions for VERA Core Physics Benchmark Progression Problem 6 demonstrated good agreement with MC21/COBRA-IE and VERA solutions to the same benchmark problem. The MC21/CTF solution for VERA Core Physics Benchmark Progression Problem 7, Watts Bar Unit 1 at HFP equilibrium xenon conditions, represents the first published coupled Monte Carlo neutronics/subchannel T-H solution for this benchmark. MC21/CTF predicts a critical boron concentration of 854.5 ppm, yielding a critical eigenvalue of 0.99994 ± 6.8E–6 (95% CI). Excellent agreement with a VERA solution of Problem 7 was demonstrated for estimated critical boron, assembly-level powers, axial power distribution, axial offset, and assembly exit temperatures. Comparisons of local pin and subchannel quantities also showed excellent agreement.

Conflicts of interest

The authors have no conflicts of interest to declare.

Acknowledgments

The Naval Nuclear Laboratory authors would like to thank the MC21 and PUMA development teams for their support during this research. Work for the Oak Ridge National Laboratory authors was funded by the DOE-sponsored “Consortium for Advanced Simulation of Light Water Reactors” (CASL) project, and ORNL research used resources of the Oak Ridge Leadership Computing Facility at the Oak Ridge National Laboratory, which is supported by the Office of Science of the U.S. Department of Energy under Contract No. DE-AC05-00OR22725. CASL research made use of the resources of the High Performance Computing Center at Idaho National Laboratory, which is supported by the Office of Nuclear Energy of the US Department of Energy and the Nuclear Science User Facility under Contract No. DE-AC07-05ID14517.

References

[1] B.N. Aviles, D.J. Kelly III, D.L. Aumiller, D.F. Gill, B.W. Siebert, A.T. Godfrey, B.S. Collins, R.K. Salko, MC21/COBRA-IE and VERA-CS multiphysics solutions to VERA core physics benchmark problem #6, Progr. Nucl. Energy (2017), http://dx.doi.org/10.1016/j.pnucene.2017.05.017.

[2] D.J. Kelly III, B.N. Aviles, P.K. Romano, B.R. Herman, N.E. Horelik, B. Forget, Analysis of select BEAVRS PWR Benchmark Cycle 1 Results using MC21 and OpenMC, Proc. PHYSOR 2014, Kyoto, Japan, September 28–October 3, 2014, American Nuclear Society (CD-ROM).

[3] N. Guilliard, W. Bernnat, J. Lapins, I. Pasichnyk, Y. Perin, K. Velkov, W. Zwermann, Analysis of large core neutronics by the Monte Carlo method coupled with thermal hydraulics, Proc. PHYSOR 2016, Sun Valley, Idaho, May 1–5, 2016, American Nuclear Society (CD-ROM).

[4] M. Daeubler, A. Ivanov, B.L. Sjenitzer, V. Sanchez, R. Stieglitz, R. Macian-Juan, High-fidelity coupled Monte Carlo neutron transport and thermal-hydraulic simulations using Serpent 2/SUBCHANFLOW, Ann. Nucl. Energy 83 (2015) 352–375.

[5] A. Ivanov, V. Sanchez, R. Stieglitz, K. Ivanov, Large-scale Monte Carlo neutron transport calculations with thermal-hydraulic feedback, Ann. Nucl. Energy 84 (2015) 204–219.

[6] D.F. Gill, D.P. Griesheimer, D.L. Aumiller, Numerical methods in coupled Monte Carlo and thermal-hydraulic calculations, Nucl. Sci. Eng. 185 (2017) 194–205.
[7] J. Leppänen, V. Hovi, T. Ikonen, J. Kurki, M. Pusa, V. Valtavirta, T. Viitanen, The numerical multi-physics project (NUMPS) at VTT technical research centre of Finland, Ann. Nucl. Energy 84 (2015) 55–62.
[8] A. Bennett, M. Avramova, K. Ivanov, Coupled MCNP/CTF code: development, testing, and application, Ann. Nucl. Energy 96 (2016) 1–11.
[9] M. Pecchia, C. Parisi, F. D'Auria, O. Mazzantini, Application of MCNP for predicting power excursion during LOCA in Atucha-2 PHWR, Ann. Nucl. Energy 85 (2015) 271–278.
[10] M. Ellis, D. Gaston, B. Forget, K. Smith, Preliminary coupling of the Monte Carlo Code OpenMC and the multiphysics object-oriented simulation environment for analyzing Doppler feedback in Monte Carlo simulations, Nucl. Sci. Eng. 185 (2017), 194–193.
[11] D. Kotlyar, E. Shwageraus, Sub-step methodology for coupled Monte Carlo depletion and thermal hydraulic codes, Ann. Nucl. Energy 96 (2016) 61–75.
[12] H. Lee, W. Kim, P. Zhang, A. Khassenov, J. Park, J. Yu, S. Choi, H.S. Lee, D. Lee, Preliminary Simulation Results of BEAVRS Three-Dimensional Cycle 1 Wholecore Depletion by UNIST Monte Carlo Code MCS, Proc. M&C 2017, Jeju, Republic of Korea, April 16–April 20, 2017, American Nuclear Society (CD-ROM).
[13] M. Lemaire, H. Lee, N. Tak, H.-C. Lee, D. Lee, Monte Carlo/thermal-fluids coupled calculations for MHTGR-350MW Benchmark, Proc. M&C 2017, Jeju, Republic of Korea, April 16–April 20, 2017, American Nuclear Society (CD-ROM).
[14] S. Liu, G. Wang, J. Liang, F. Yang, Z. Chen, X. Guo, Q. Wu, J. Guo, Y. Qiu, X. Tang, Z. Li, K. Wang, RMC capability of multi-cycle HFP full core burnup simulation, Proc. M&C 2017, Jeju, Republic of Korea, April 16–April 20, 2017, American Nuclear Society (CD-ROM).
[15] D.P. Griesheimer, D.F. Gill, B.R. Nease, T.M. Sutton, M.H. Stedry, P.S. Dobreff, D.C. Carpenter, T.H. Trumbull, E. Caro, H. Joo, D.L. Millman, MC21 v.6.0–A continuous-energy Monte Carlo particle transport code with integrated reactor feedback capabilities, Ann. Nucl. Energy 82 (2015) 29–40.
[16] R. Salko, M. Avramova, CTF Theory Manual, Reactor Dynamics and Fuel Management Group, Pennsylvania State University, 2014.
[17] M. Sieger, VERA 3.3 Release Notes, CASL Technical Report: CASL-U-2015-0042-000, 2015.
[18] B. Kochunas, D. Jabaay, S. Stimpson, A. Graham, T. Downar, B. Collins, K.S. Kim, W. Wieselquist, K. Clarno, J. Gehin, VERA Core Simulator Methodology for PWR Cycle Depletion, CASL Technical Report: CASL-U-2015-0155-000, 2015.
[19] A. Godfrey, VERA Core Physics Benchmark Progression Problem Specifications, Revision 4, CASL Technical Report: CASL-U-2012-0131-004, 2014.
[20] D.L. Aumiller, G.W. Swartele, M.J. Meholic, L.J. Lloyd, F.X. Buschman, COBRA-IE: A New Sub-channel Analysis Code, Proc. NURETH-16, Chicago, Illinois, August 30–September 4, 2015, American Nuclear Society (2015) (CD-ROM).
[21] S. Palmtag, A. Godfrey, VERA Common Input User Manual, CASL Technical Report: CASL-U-2014-0014-002, 2014.
[22] D.J. Kelly III, T.M. Sutton, T.H. Trumbull, P.S. Dobreff, MC21 Monte Carlo analysis of the Hoogenboom-Martin Full-Core PWR Benchmark Problem, Proc. PHYSOR 2010, Pittsburgh, Pennsylvania, May 9–May 14, 2010, American Nuclear Society (2010) (CD-ROM).
[23] R. Salko, Development of CTF Capability for Modeling Reactor Operating Cycles with Crud Growth, CASL Technical Report: CASL-U-2014-0188-000, 2014. J. GLEASON, Format for a Report, ANS-2008, American Nuclear Society, 2008.